Giant photoinduced Faraday rotation due to the spin-polarized electron gas in an *n*-GaAs microcavity

R. Giri, S. Cronenberger, M. Vladimirova, and D. Scalbert
Laboratoire Charles Coulomb, Unité Mixte de Recherche 5221 CNRS/UM2, Université Montpellier 2, Place Eugene Bataillon, 34095 Montpellier Cedex 05, France

K. V. Kavokin and M. M. Glazov
Ioffe Physical-Technical Institute of the Russian Academy of Sciences, 26, Politechnicheskaya, 194021 Saint Petersburg, Russia

M. Nawrocki
Institute of Experimental Physics, Faculty of Physics, Warsaw University, Hoża 69, 00-681 Warsaw, Poland

A. Lemaître and J. Bloch
Laboratoire de Photonique et de Nanostructures, Unité Propre de Recherche du CNRS, Route de Nozay, 91460 Marcoussis, France
(Received 20 September 2011; revised manuscript received 22 February 2012; published 10 May 2012)

Faraday rotation up to 19° in the absence of an external magnetic field is demonstrated in an *n*-type bulk GaAs microcavity under circularly polarized optical excitation. This strong effect is achieved because (i) the spin-polarized electron gas is an efficient Faraday rotator and (ii) the light wave makes multiple round trips in the cavity. We introduce a concept of Faraday rotation cross section as a proportionality coefficient between the rotation angle, electron spin density and optical path and calculate this cross section for our system. From independent measurements of photoinduced Faraday rotation and electron spin polarization we obtain quantitatively the cross section of the Faraday rotation induced by free electron spin polarization $\sigma_F^{\rm exp} = -(2.5 \pm 0.6) \times 10^{-15}$ rad×cm^2 for photon energy 18 meV below the band gap of GaAs, and electron concentration 2×10^{16} cm^{-3}. It appears to exceed the theoretical value $\sigma_F^{\rm th} = -0.7 \times 10^{-15}$ rad×cm^2, calculated without fitting parameters. We also demonstrate the proof-of-principle of a fast optically controlled Faraday rotator.

DOI: 10.1103/PhysRevB.85.195313 PACS number(s): 78.66.Fd, 78.20.Ls, 78.47.D−, 78.20.Fm

I. INTRODUCTION

The rotation of the polarization plane of light upon transmission through transparent media, either magnetized or subjected to a magnetic field, is known as Faraday effect.[1] Faraday rotation has been demonstrated in a wide range of materials,[2] from paramagnetic glasses to interstellar media,[3] and has important applications such as Faraday rotators, optical isolators, and circulators.[4] The efficiency of the material in producing Faraday rotation is characterized by the Verdet constant V, such that the Faraday rotation angle $\theta_F = VBd$, where B is the applied magnetic field, d is the sample thickness. By convention, the sign of the Verdet constant is positive, if the rotation is clockwise for the observer looking in the direction of the magnetic field.[5]

In semiconductors, two main contributions to the Faraday rotation are related to two distinct polarization-sensitive optical transitions mechanisms: free carriers or Drude transitions (far in the transparency region) and interband (or excitonic) transitions close to the fundamental absorption edge.[6–11] Verdet constants in nonmagnetic materials, such as semiconductors, are normally small.[11] It is also known that Faraday rotation can change its sign in the vicinity of absorption edge in some semiconductors, such as GaAs.[9,12] In contrast, semiconductors doped with magnetic impurities (e.g., GaMnAs, CdMnTe) produce strong Faraday rotation.[5,13] In these diluted magnetic semiconductors the *sp-d* exchange interaction between the magnetic ion *d* states on one hand and the conduction and valence band states on the other hand is responsible for giant spin splittings of electronic states and strong enhancement of the interband Faraday rotation.

Another way to produce Faraday rotation in semiconductors is optical orientation of carrier spins.[14] Under quasiresonant pumping with circularly polarized light, electron spin polarization up to 50% in bulk semiconductors can be achieved. Under these conditions the Faraday rotation is expected to be proportional to the spin polarization of the electron gas and the thickness of the spin-polarized area.[15] Because the latter is usually limited by the absorption length and quite small, the experimentally observed values of Faraday rotation are of the order of milliradian.[16]

In this work we use a planar optical cavity to increase the Faraday rotation induced by the optically polarized electron gas. This idea has already been fruitfully employed to study Faraday rotation in quantum wells embedded in a microcavity, where polarization was induced either by magnetic field[17] or by optical pumping.[18] The enhancement of Faraday rotation in a microcavity is due to multiple round trips of the light between the mirrors. The number of round trips is given by $N = Q\lambda_{\rm res}/(4\pi L)$, where Q, L, and $\lambda_{\rm res}$ are respectively the cavity quality factor, the thickness, and the resonance wavelength inside the cavity, and it is quite large, $N > 10^3$, in the high finesse cavities, as a rule.

In the case of optical pumping the efficiency of spin-polarized electrons to rotate the polarization plane is not adequately characterized by the Verdet constant. Instead, in this paper we employ the Faraday rotation cross section σ_F,

such that

$$\theta_F = \sigma_F S_z d, \tag{1}$$

where $S_z = \frac{1}{2}(n_\uparrow - n_\downarrow)$ is the electron spin density, and $n_\uparrow$ ($n_\downarrow$) is the density of spin up (spin down) electrons in the direction of propagation. By analogy with the definition of field induced Faraday rotation, we adopt the convention that rotations, which are clockwise for the observer looking along the direction of spin polarization, are positive.

Here we study the photoinduced Faraday rotation in a bulk n-doped microcavity. In the same sample we measure independently Q, the degree of photoinduced polarization of the electron gas ρ_e and the photoinduced rotation angle θ_F. This allows us to determine σ_F quantitatively and to compare it with the theoretical prediction. Finally, we demonstrate that Faraday rotation induced by the the pump beam can be quite fast: in our experiments the rotation of 10° is achieved in 70 ns, but it can be much shorter and is ultimately limited by the rise time of the optical pulse.

The paper is organized as follows: In Sec. II we present the sample and the experimental configuration used for the three different variants of photoinduced Faraday rotation experiments realized in this work. Namely, continuous wave Faraday rotation (cw-FR) and electron spin lifetime measurement by Hanle effect [Fig. 2(a)]; determination of electron spin polarization from nuclear spin cooling experiments [Fig. 2(b)]; time-resolved Faraday rotation (TRFR) under pulsed excitation [Fig. 2(c)]. The results of photoinduced Faraday rotation experiments and measurements of electron spin lifetime by Hanle effect are described in Sec. III. The spin polarization measurements by nuclear spin cooling are presented in Sec. IV. In this section results of polarization-resolved photoluminescence are also reported, in order to check the results obtained by nuclear spin cooling. In Sec. V we introduce the Faraday rotation cross section, give an expression of this quantity within a microscopic model, and then determine its value experimentally. Section VI describes the time-resolved experiments, which provide the proof-of-principle demonstration of optically pumped Faraday rotator. This is followed by discussion and conclusion (Sec. VII).

II. EXPERIMENT

Figure 1 shows the microcavity structure used in this study and the corresponding transmission spectrum calculated using transfer matrix method. The sample is a 3581-Å thick Si-doped GaAs cavity sandwiched between two Bragg mirrors, consisting of 25(30) AlAs/$Al_{0.1}Ga_{0.9}As$ pairs for the upper (bottom) mirrors. The density of the electron gas in the cavity layer is $n_e = 2 \times 10^{16}$ cm^{-3}. The sample is grown on a 400-μm thick undoped GaAs substrate. The molecular beam epitaxy grown cavity was wedge shaped in order to have the possibility to tune the cavity mode energy by varying the spot position on the sample. However, the wedge was small enough to not compromise the measurement of the high Q-factor of the cavity. The detuning between the energy gap of undoped GaAs, chosen as a reference, and the cavity mode could thus be varied between 16 and 22 meV. The sample was cooled down to the temperature range from 2 K to 20 K either in a helium bath or in a cold finger cryostat. The three variants of

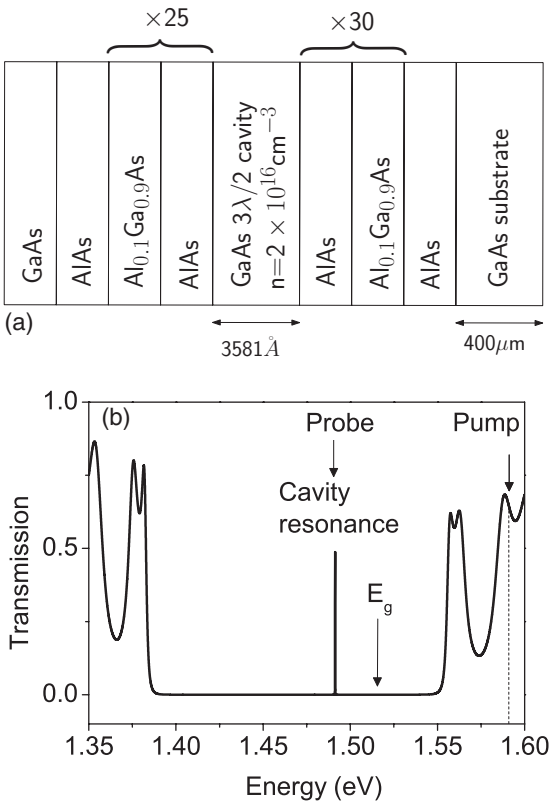

FIG. 1. (a) The n-doped GaAs microcavity sample with substrate used in this study (a) and the calculated transmission spectrum of the cavity. (b) We pumped at an energy of 1.59 eV and probed at the cavity resonance, about 18 meV below the band gap.

the pump-probe setup used for measurement of cw-FR and Hanle effect, nuclear spin cooling and TRFR are shown in Fig. 2. In the three variants the pump beam is delivered by a cw-laser diode emitting at 780 nm eventually chopped by an acousto-optic modulator with switching time of 10 ns. The probe laser is either a cw-Al_2O_3:Ti laser or a pulsed Al_2O_3:Ti laser delivering 80 fs pulses. The diameter of both laser spots on the samples were about 50 μm.

The first variant of experimental setup [Fig. 2(a)] was used to measure the cw-FR and the Hanle effect. Optical spin orientation of the electrons was achieved with a photoelastic modulator (PEM) modulating the circular polarization of the pump at the frequency $f = 50$ kHz in order to avoid the dynamic nuclear polarization by the optically oriented electrons. The spin polarization of photoexcited electrons is partly transferred to the electron gas, which gets polarized and induces a modulated Faraday rotation of the probe beam $\theta_F(t) = \theta_0 \sin(2\pi f t)$. The Faraday rotation was detected with a linear polarization analyzer and a photodiode. The total intensity seen by the detector can be developed in a Fourier series $I(t) = I_0(t)[\frac{1}{2} + J_1(2\theta_0) \sin(2\pi f t) + \text{odd harmonics of f}]$, where $I_0(t)$ is the transmitted probe intensity modulated by the chopper at frequency f_c, and the analyzer is set at 45° with respect to the transmitted probe polarization plane (when $\theta_0 = 0$) for maximum Faraday rotation signal. In our experiments $\theta_F \leqslant 19°$ and the error made in replacing $J_1(2\theta_0)$ by θ_0 is less than 6%. Thus simultaneous demodulation of the signal at frequencies f and f_c yields $\theta_0 = CI_f/I_{f_c}$, where the

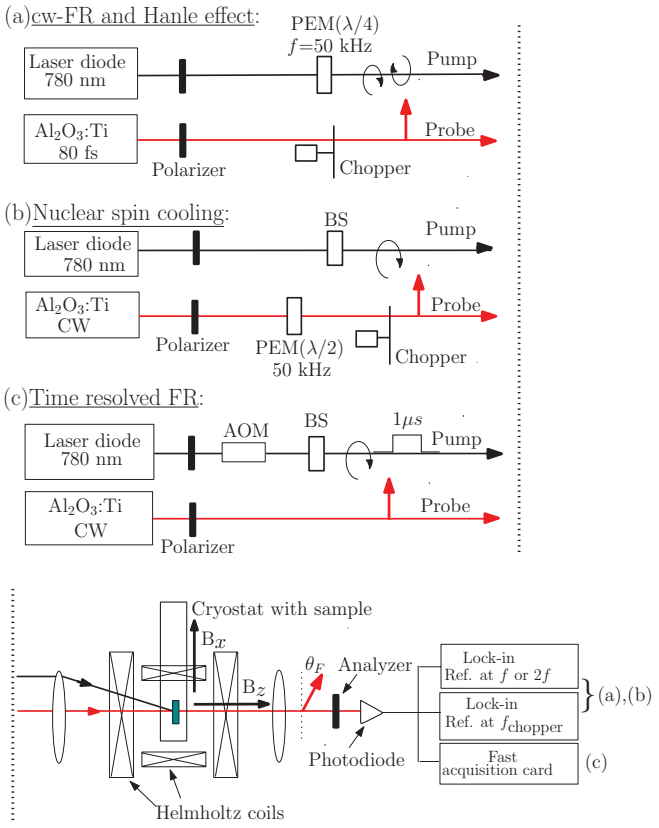

FIG. 2. (Color online) The three variants of the setup used in photoinduced Faraday rotation experiments (PEM: photoelastic modulator; BS: Babinet-Soleil compensator; AOM: acousto-optic modulator). Upper panel: (a) cw-Faraday rotation and Hanle effect; (b) nuclear spin cooling for measurement of the Knight field; and (c) time-resolved Faraday rotation induced by microsecond long pulses. Lower panel: cryostat, Helmholtz coils used to apply longitudinal and/or transverse magnetic field, and detection setup used is common in all three variants.

calibration factor is determined experimentally by rotating the analyzer by a known angle.

A transverse magnetic field causes depolarization of the electron spin (Hanle effect), which reduces θ_F. The spin relaxation time of the electrons is extracted from the Hanle curves, as discussed in Sec. III.

The second variant of the setup [Fig. 2(b)] was used to measure the Knight field induced by the spin polarized electron gas and acting on nuclear spins. Since the Knight field is proportional to the electron spin polarization, measurement of the Knight field provides information about the electron spin polarization density. Here we used a Babinet-Soleil compensator to set a fixed pump polarization (either σ^+ or σ^-) and the linearly polarized cw-Ti:Sapphire laser was used as the probe. In this variant the linear probe polarization is modulated with the PEM set at a retardance of $\lambda/2$, and the Faraday rotation signal is extracted by demodulation at $2f$.

The third variant [Fig. 2(c)] was used for time-resolved measurement of the Faraday rotation induced by a pump pulse. Microsecond long pulses, with polarization set either as σ^+ or σ^-, rise time and decay time of about 10 ns, are shaped from the cw-laser diode by an acousto-optic modulator (AOM). The buildup of electron spin polarization during pumping and its decay after the pump is switched off are monitored via Faraday rotation $\theta_F(t)$ of the probe beam delivered by cw-Al_2O_3:Ti laser. The intensity recorded by the detector $I(t) = I_0(t)(\frac{1}{2} + \theta_F(t))$ is measured in this case with a fast acquisition card sampling the signal at 200 MHz.

III. PHOTOINDUCED FARADAY ROTATION AND ELECTRON SPIN RELAXATION TIME

The Faraday rotation and the depolarization of Faraday rotation by a transverse magnetic field B_x applied along x axis (Hanle effect) are measured at 2 K with pump power varying between 3 μW and 1 mW. The pump laser is focused on a 50-μm spot diameter. The spin relaxation time is extracted from the Hanle curves measured at different pump powers. The Hanle effect detected via photoluminescence has been routinely used to measure spin relaxation time of electrons in semiconductors.[14] Here we detect the depolarization of the electron spin via Faraday rotation.[16,19] The reduction of the electron spin polarization, and thus of θ_F, in a transverse magnetic field is described by the Lorentz curve

$$\theta_F(B) \propto \frac{1}{1 + (g_e \mu_B B_x T_s/\hbar)^2}, \tag{2}$$

where μ_B is the Bohr magneton, T_s is the electron spin lifetime and g_e is the electron g factor.

In case of the n-doped semiconductor, the effective spin lifetime is given by $1/T_s = 1/\tau_s + G/n_e$, where τ_s is the electron spin relaxation time, n_e is the concentration of equilibrium electrons and G is the carrier generation rate.[20] The full width at half maximum (FWHM) of the Lorentz curve $B_{\mathrm{FWHM}} = (2\hbar/g_e \mu_B T_s)$, is inversely proportional to the spin lifetime. This allows for the measurement of the spin lifetime and, by extrapolation to $G = 0$, the spin relaxation time.

Figure 3(a) shows the photoinduced Faraday rotation as a function of the pump power density. One can see that Faraday rotation increases sublinearly with power and at saturation exceeding 10°. Figure 3(b) shows the FWHM of the Hanle curves as a function of the pump power density. Using the same procedure as Dzhioev,[20] we deduce a spin relaxation time of 160 ns, close to the value reported by Crooker[16] for the same electron concentration.

To understand the saturation of θ_F with pump power, we note that in the spin-polarized electron system it is proportional to electron spin density, S_z.[15] In our experiments the spin density of photogenerated electrons is much smaller than the resident electron density n_e, hence, the electron spin polarization degree $\rho_e = (n_\uparrow - n_\downarrow)/(n_\uparrow + n_\downarrow)$, where $n_\uparrow$ ($n_\downarrow$) is the density of electrons with spin in the direction of (opposite to) the light propagation direction, can be related with electron spin density as

$$\rho_e = \frac{2S_z}{n_e}. \tag{3}$$

Therefore, the Faraday rotation is proportional to the spin polarization of the electron gas

$$\theta_F = \mu \rho_e. \tag{4}$$

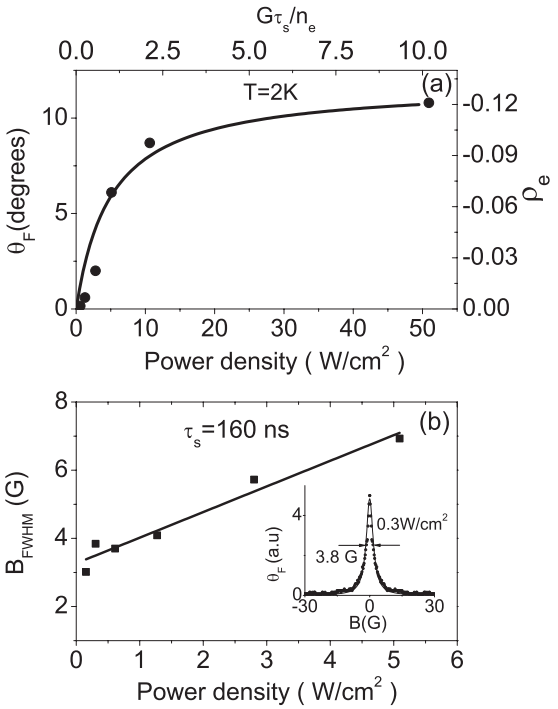

FIG. 3. (a) Left scale: cw-Faraday rotation as function of the pump power (closed circles). Right scale: electron polarization calculated with Eq. (5) plotted as a function of $G\tau_s/n_e$ (solid line). (b) The full width at half maximum of the Hanle curves versus pump power density. Extrapolation to zero pump power density gives $B_{\mathrm{FWHM}} = 3.3$ G, corresponding to spin relaxation time of 160 ns. Inset shows the Hanle curve acquired at 0.3 W/cm^2.

The proportionality factor μ will be determined experimentally in the next section, and used later (Sec. V) to determine the Faraday rotation cross section.

From the rate equations for spin-up and spin-down electron densities in the presence of optical pumping and recombination, and assuming that the excess carrier recombination time is shorter than the electron spin relaxation time τ_s one gets

$$\rho_e = \rho_i G\tau_s/(n_e + G\tau_s), \tag{5}$$

where ρ_i is the initial spin polarization of photoexcited carriers after they have thermalized to the bottom of the conduction band. Since the initial kinetic energy of the carriers is relatively large, of the order of 75 meV, they are likely to be partially depolarized before they thermalize,[21] so that $\rho_i < 0.5$. We note that similar to classical optical orientation experiments in bulk semiconductors, the holes are assumed to be completely depolarized almost immediately after photoexcitation.

In Fig. 3(a) the angle of Faraday rotation measured as a function of power is compared to the calculation by means of Eq. (5). Here we used the independently measured value of the electron spin polarization $\rho_e = 0.11$ at 50 W/cm^2 (see next section) and $\tau_s = 160$ ns (see above). In calculating the generation rate G, we assumed absorption coefficient $\alpha = 10^4$ cm^{-1} Ref. 22, the reflection coefficient $R = 0.5$, and 50 μm spot diameter. One can see that the observed saturation of Faraday rotation is, indeed, well reproduced by the saturation of ρ_e and therefore S_z.[23]

IV. DETERMINATION OF ELECTRON SPIN POLARIZATION

Because of the large negative detuning of the cavity mode in our sample with respect to the GaAs energy gap, the interband emission is strongly suppressed. Therefore, direct determination of electron spin polarization from the degree of circular polarization of photoluminescence was not possible. For this reason we started with an indirect method based on the cooling of the nuclear spin system in the electron (Knight) field[14,24,25] (Sec. IV A). We have also measured the degree of polarization of electron gas from the polarized photoluminescence (PL) experiments, but in order to enable the detection of interband emission, the upper Bragg mirror was etched from the microcavity sample (Sec. IV B). Note, however, that this may affect the measured spin polarization for several reasons, such as degradation of the sample quality, and change in the probability of photon recycling.

A. Measurement of the knight field

Under steady state optical pumping conditions in the external field $\boldsymbol{B}$, the reciprocal nuclear spin temperature ($\beta_N = 1/k_B T_N$) can be expressed as[14]

$$\beta_N = \frac{4I}{\mu_I} \frac{(\boldsymbol{B} + \boldsymbol{B}_e)\cdot \boldsymbol{S}/n_e}{(\boldsymbol{B} + \boldsymbol{B}_e)^2 + \xi B_L^2}, \tag{6}$$

where I and μ_I are the nuclear spin and nuclear magneton respectively, $\boldsymbol{B}_e = 2b_e\boldsymbol{S}/n_e$ is the electron field (Knight field) exerted by the electrons on the nuclei, $\boldsymbol{S}$ is the electron spin density, b_e is the value of the Knight field at saturation of electron spin polarization, B_L is the nuclear local field and ξ is a numerical coefficient which depends on the type of spin-spin interaction.

For delocalized electrons

$$b_e = \frac{8\pi}{3I} n_e \mu_B \eta, \tag{7}$$

where I is the nuclear spin, and $\eta = |u(0)|^2$ with $u(0)$ being the amplitude of the Bloch function at the either Ga or As site. Since these amplitudes are different at the Ga and As sites, so saturation Knight field b_e is different as well. We take $\eta_{\mathrm{Ga}} = 2.7 \times 10^3$ and $\eta_{\mathrm{As}} = 4.5 \times 10^3$ Ref. 26, and obtain $b_e^{\mathrm{Ga}} = 2.8$ G and $b_e^{\mathrm{As}} = 4.6$ G. We introduce effective saturation Knight field which, in first approximation reads $b_e = (b_e^{\mathrm{Ga}} + b_e^{\mathrm{As}})/2 = 3.7$ G. One can see from Eq. (6) that the nuclear spin temperature depends strongly on $\boldsymbol{B} + \boldsymbol{B}_e$ and becomes infinite when the external field compensates the Knight field ($\boldsymbol{B} + \boldsymbol{B}_e \to 0$). Measurements of the nuclear spin temperature as a function of $\boldsymbol{B}$ allow for the determination of the Knight field compensation conditions and thus the average electron spin $\boldsymbol{S}$.

These measurements were done with the second variant of the setup shown in Fig. 2(b). We proceed in two stages as shown in Fig. 4(a). First, the nuclear spin system is cooled down by optical pumping (pump power is 500 μW) in a longitudinal field $\boldsymbol{B} \parallel z$, $|\boldsymbol{B}| = B_z$ during few minutes. This is the cooling stage. Then, during the measurement stage, B_z is switched off and a small transverse field $B_x = 1.5$ G $\div$ 2.5 G is switched on. The pump power is set to 85 μW, weak enough to avoid any repolarization of the nuclei during this stage.

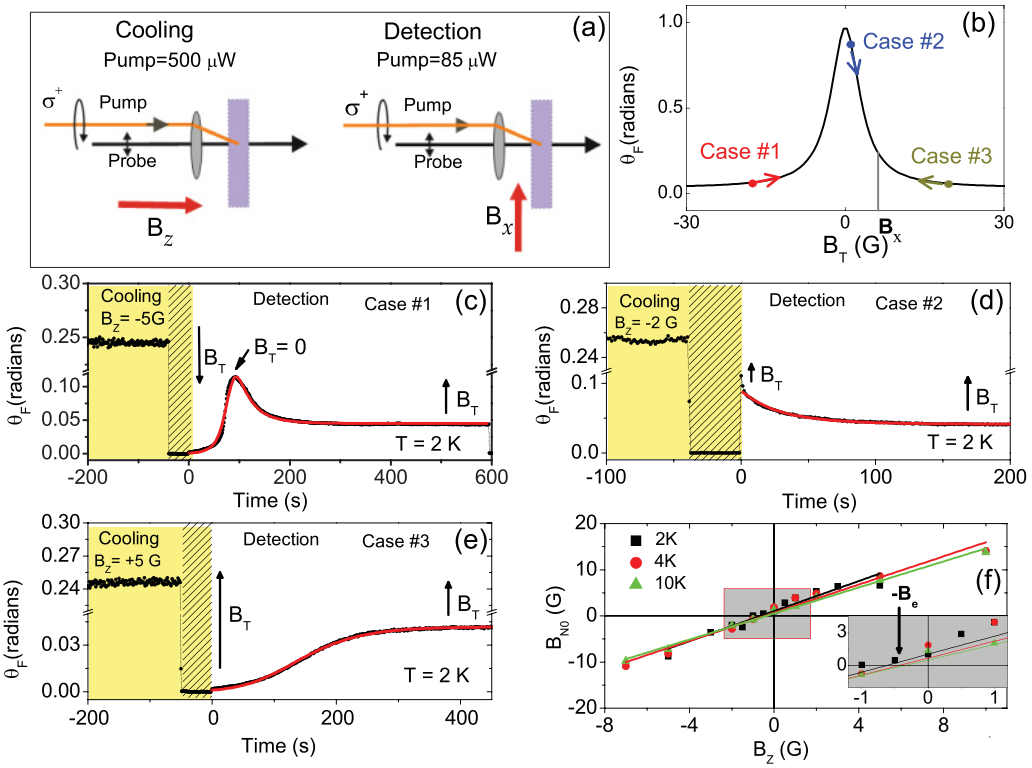

FIG. 4. (Color online) (a) Scheme for optical cooling of nuclear spins at relatively large pump power in a longitudinal field (left) and detection in a small transverse field at lower pump power (right). (b) Typical Hanle curve versus total field $B_T = B_N + B_x$. Depending on the initial value of B_T, Faraday rotation will exhibit different time evolutions as B_T relaxes to B_x. (c)–(e) Time evolution of Faraday rotation during cooling in a longitudinal field (yellow region), and detection in a weak transverse field B_x =1.5 G, for the three cases shown in panel (b) (red curves are fit to the data using Eq. (8)). In the shaded area (during cooling) the signal was not recorded to allow for a change in the lock-in sensitivity. (f) The extracted nuclear field as a function of longitudinal field. The observed Knight field of about 0.4 G is independent of sample temperature.

According to the Eq. (6), if an appreciable cooling is achieved during the cooling stage, then, depending on the sign and value of both B_z and B_e, the nuclei will repolarize either parallel ($\beta_N < 0$) or antiparallel ($\beta_N > 0$) to the transverse field B_x, creating an effective nuclear (Overhauser) field B_N acting on the electrons. If during the cooling stage the external field is such that it compensates the Knight field ($\boldsymbol{B} \approx -\boldsymbol{B}_e$) then nuclear cooling is not possible and $B_N \approx 0$, $\beta_N = \infty$.

The total transverse field experienced by electrons $B_T = B_x + B_N$. The presence of transverse field leads to a measurable modification of the electron spin polarization, with respect to the polarization created by the pump. As long as the nuclear spin system heats up, electron spin polarization varies with time. It follows a part of the Hanle curve from $B_T = B_x + B_N$ to $B_T = B_x$ when B_N is fully relaxed [Fig. 4(b)]. The resulting electron spin polarization was monitored by the Faraday rotation of the probe beam, as shown in Fig. 2(b).

Different kinds of depolarization curves [Figs. 4(c)–4(e)] can be observed depending on the initial value of the total field. If $B_T < 0$ [Fig. 4(c)], the electron spin polarization as well as Faraday rotation angle θ_F first increase, goes through a maximum when $B_T = 0$, then decreases as B_T decreases toward B_x due to nuclear spin relaxation processes. If $0 < B_T < B_x$, then θ_F monotonously decreases [Fig. 4(d)]. These two cases will eventually occur when B_N and B_x are antiparallel (i.e., for positive nuclear temperatures $\beta > 0$). Finally (case 3), if $B_T > B_x$ (which takes place for negative nuclear temperatures $\beta_N < 0$), Faraday rotation angle θ_F increases steadily as B_T decreases toward B_x [Fig. 4(e)].

Assuming that the nuclear field decays exponentially, the time evolution of Faraday rotation can be expressed as

$$\theta_F(t) \propto \left[1 + \left(\frac{B_x + B_{N_0} e^{-t/T_1}}{B_{\mathrm{FWHM}}/2}\right)^2\right]^{-1}, \qquad (8)$$

where B_{N_0} is the initial nuclear field, T_1 is the longitudinal nuclear spin relaxation time. Figures 4(c)–4(e) show the fits of the data using this expression, from which we deduce B_{N_0} for each value of B_z. The resulting values of B_{N_0} for each B_z are shown in Fig. 4(f). One can see in the inset of Fig. 4(f), that the field B_z at which B_{N_0} passes through zero is slightly shifted from zero. This is a direct evidence that the nuclei get polarized in the Knight field created by the electrons, even without external field. From this shift we estimate $B_e = (0.4 \pm 0.1)$ G, which gives an average electron spin polarization $\rho_e = (11 \pm 3)\%$. At the same pump power $P = 500$ μW, corresponding to an intensity of 25 W/cm^2, we measured $\theta_F = 10^\circ$, hence, from Eq. (4) $\mu = \theta_F/\rho_e = -100^\circ \pm 25^\circ$.

B. Polarized photoluminescence

The measurements of electron spin polarization from the polarized photoluminescence (PL) were done on the piece of the sample, where the upper Bragg mirror was chemically etched. The excitation energy was 1.59 eV, which corresponds to the energy of the pump in the Faraday rotation experiments. The excitation intensity was modulated at about 300 Hz and the PEM was used to modulate the polarization between σ^+ and σ^- at 50 kHz. The photoluminescence was collected, passed through a circular polarization analyzer, and then a grating spectrometer. A photomultiplier tube connected with two lock-in amplifiers was used to extract the signal. One lock-in amplifier operated synchronously with the PEM to detect the differential signal $(I^+ - I^-)$ and the other lock-in operated synchronously with the optical chopper to provide the total signal $(I^+ + I^-)$. Then the degree of circular polarization of the luminescence $\rho_c = (I^+ - I^-)/(I^+ + I^-)$, where I^+ and I^- are the intensity of the σ^+ and σ^- polarized PL respectively.

Figure 5 shows the measured PL intensity and polarization. The broad PL spectrum and the characteristic step in the circular polarization seen on the higher energy tail of the spectrum are typical of degenerate semiconductors.[20]

Assuming a Fermi distribution of the electrons in a parabolic band, as well as a flat dispersion of valence band, the PL intensity reads

$$I(E) \propto \frac{\mathcal{D}(E)}{1 + e^{\beta_e(E-E_F)}}, \tag{9}$$

where $\beta_e = 1/k_B T_e$ is the inverse electron temperature, E_F is the Fermi energy, and $\mathcal{D}(E) \propto E^{1/2}$ is the density of states of the conduction band. If the average electron spin S_z is small enough then by differentiating the thermal distribution function we obtain the degree of circular polarization as

$$\rho_c(E) \simeq \frac{\frac{1}{3}\beta_e E_F S_z}{1 + e^{-\beta_e(E-E_F)}}. \tag{10}$$

At low energy the polarization goes to zero, while at high energy the PL polarization degree tends to

$$\rho_c^{\infty} = \tfrac{1}{3}\beta_e E_F S_z. \tag{11}$$

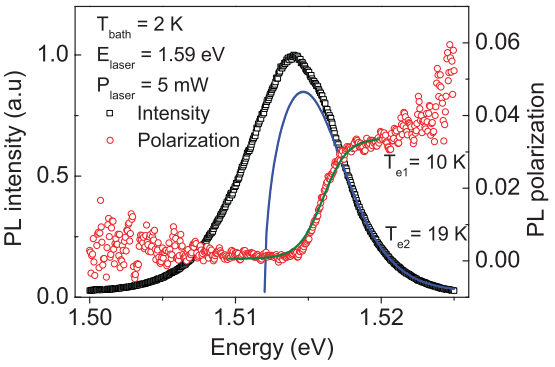

FIG. 5. (Color online) The spectrum of PL intensity (open square) and the PL circular polarization from the GaAs microcavity (open circle). The solid lines are fit by the calculated PL intensity and electron spin polarization assuming Fermi distributions of electrons.

From the fit of the PL intensity (polarization) with Eq. (9) [Eq. (10)] we get the electron gas temperature $T_{e1} = 10$ K ($T_{e2} = 19$ K), and $\rho_c^{\infty} = 0.03$. The different electron temperatures deduced from PL intensity and polarization indicate that the interband emission model used here is too simple. Indeed the observed spectrum is relatively complicated and contains at least two components. However these fits give an estimate of the electronic temperature in the range 10–20 K. From Eq. (11) with $E_F = 4$ meV, we deduce the electron gas spin polarization degree $\rho_e = 6 \pm 2\%$, in reasonable agreement with the value estimated from the Knight field.

V. FARADAY ROTATION CROSS SECTION

A. Definition

In nonmagnetic media Faraday rotation induced by an external magnetic field applied along the light beam is usually characterized by the Verdet constant, which is the Faraday rotation angle per unit traveling length in the medium, and per unit magnetic field. In case of photoinduced Faraday rotation the magnetic field is absent, hence, this description is not appropriate, and it is more convenient, and physically sound, to introduce the concept of Faraday rotation cross section σ_F, in analogy with other more familiar cross sections. If one considers linearly polarized light propagating along z direction, and interacting with a single particle with spin projection $+\hbar$ in this direction, then σ_F is defined as the induced Faraday rotation per unit surface of the beam cross section. Hence, for a medium containing a large number of spins with average spin density S_z and effective thickness d_{eff}, the Faraday rotation is simply given by

$$\theta_F = \sigma_F S_z d_{\text{eff}}. \tag{12}$$

If we assume that a given spin density produces the same Faraday rotation, whether it is induced optically or by a magnetic field, then by identification the Verdet constant is merely proportional to the Faraday rotation cross section, the proportionality factor being the spin susceptibility. We will see, however, in Sec. V C2 that such assumption is not valid, in general, for conduction band electrons.

B. Calculation

In order to calculate the Faraday rotation induced by spin-polarized electrons in bulk semiconductor we follow the theoretical model of Aronov and Ivchenko,[15] and calculate first the contribution related with the state-filling effects. We introduce the frequency-dependent dielectric susceptibilities $\varepsilon_{\pm}(\omega)$ for σ^+ and σ^- polarized light waves propagating in the positive direction of z axis. In the vicinity of the band edge ($\hbar\omega < E_g$) the real part of this difference can be written as[27]

$$\mathrm{Re}\{\varepsilon_+ - \varepsilon_-\} = \frac{4\pi e^2}{m_0^2 \hbar\omega^2 \Omega} \frac{|p_{cv}|^2}{3} \sum_{\boldsymbol{k}} \left(\frac{f_{1/2}(k) - f_{-1/2}(k)}{\omega - E_g/\hbar - \hbar k^2/2\mu_{hh}} + \frac{f_{1/2}(k) - f_{-1/2}(k)}{\omega - E_g/\hbar - \hbar k^2/2\mu_{lh}} \right). \tag{13}$$

Here m_0 is free electron mass, Ω is the normalization volume, p_{cv} is the interband momentum matrix element, μ_{hh} (μ_{lh}) is

the reduced electron-heavy hole (electron-light hole) mass, and $f_{\pm 1/2}(k)$ are the distribution functions of electrons with spin projections $\pm 1/2$ onto the z axis. The Faraday rotation angle can be written as

$$\theta_F = \frac{\omega}{4cn}\,\mathrm{Re}\{\varepsilon_- - \varepsilon_+\} d_{\mathrm{eff}}, \tag{14}$$

where n is the background refractive index.

We introduce the electron spin density as

$$S_z = \frac{1}{V}\sum_{\boldsymbol{k}} s_z(\boldsymbol{k}), \tag{15}$$

where

$$s_z(\boldsymbol{k}) = [f_{1/2}(\boldsymbol{k}) - f_{-1/2}(\boldsymbol{k})]/2.$$

In degenerate electron gas with low electron spin polarization the spin distribution function is proportional to $\delta(E_k - E_F)$ and summation over the wave vector $\boldsymbol{k}$ in Eq. (13) becomes simple. Using Eq. (12) we finally obtain

$$\sigma_F^{\mathrm{sf}} = -\frac{\pi e^2\hbar}{3mcn}\left(\frac{1}{E_g + \frac{m}{\mu_{hh}}E_F - \hbar\omega} + \frac{1}{E_g + \frac{m}{\mu_{lh}}E_F - \hbar\omega}\right), \tag{16}$$

where $|p_{cv}|^2/m_0$ was related with the effective electron mass m.

In the spin-polarized electron gas the exchange interaction between electrons renormalizes their energies depending on spin orientation. The energy shift is different for $s_z = +1/2$ and $s_z = -1/2$ electrons, hence Hartree-Fock effect can be understood as interaction-induced effective magnetic field acting on electron spins.[28] This effective field can be written as[29]

$$\Delta_{\mathrm{HF}}(\boldsymbol{k}) = -2\sum_{\boldsymbol{k}'} V_{\boldsymbol{k}'-\boldsymbol{k}} s_z(\boldsymbol{k}), \tag{17}$$

where $V_{\boldsymbol{q}} = 4\pi e^2/[V\varkappa(q^2 + q_{\mathrm{TF}}^2)]$ is the Fourier transform of electron-electron interaction potential with $q_{\mathrm{TF}} = \sqrt{6\pi N e^2/\varkappa E_F}$ being Thomas-Fermi screening wave vector and $\varkappa$ being background static dielectric constant. For the sake of estimation one can neglect the wave-vector dependence of Δ_{HF} and take its value of $|\boldsymbol{k}| = k_F$. Therefore, the Hartree-Fock effect on photoinduced Faraday rotation can be evaluated similarly to the calculation of the magnetic field-induced Faraday rotation[10] and Faraday rotation caused by nuclei in semiconductors[30] with the result [cf. Ref. 29 where two-dimensional case is considered]

$$\sigma_F^{\mathrm{HF}} = -\frac{e^2\hbar}{48mcn}\frac{\mathcal{U}_{k_F}}{\sqrt{E_g - \hbar\omega}} \times\left[\left(\frac{2\mu_{hh}}{\hbar^2}\right)^{3/2}\left(1 - \frac{2}{\pi}\arctan\sqrt{\frac{\frac{m}{\mu_{hh}}E_F}{E_g - \hbar\omega}}\right) + \left(\frac{2\mu_{lh}}{\hbar^2}\right)^{3/2}\left(1 - \frac{2}{\pi}\arctan\sqrt{\frac{\frac{m}{\mu_{lh}}E_F}{E_g - \hbar\omega}}\right)\right], \tag{18}$$

where

$$\mathcal{U}_k = \frac{\Delta_{\mathrm{HF}}(k_{\mathrm{F}})}{S_z} = -\frac{2\pi e^2}{\varkappa k_F}\ln\left(1 + \frac{4k_F^2}{q_{\mathrm{TF}}}\right). \tag{19}$$

It is worth noting that the spectral behavior of the spin signals caused by the state-filling and Hartree-Fock effects is different. At relatively high detunings, $\Delta = E_g - \hbar\omega \gg E_F$, the $\sigma_F^{\mathrm{sf}} \propto \Delta^{-1}$, while Hartree-Fock contribution behaves as $\sigma_F^{\mathrm{HF}} \propto \Delta^{-1/2}$. In the vicinity of the absorption edge, the singularity in the state-filling contribution, σ_F^{sf}, is smeared due to the electron scattering, which results in the broadening of the edge.

Figure 6(a) shows the ratio of the Hartree-Fock and state-filling contributions to the Faraday rotation cross section. It follows from Eqs. (16) and (18) that σ^{HF} and σ^{sf} have opposite signs. Their ratio is controlled by the following parameters: ratio of the Fermi energy and interaction energy $\mathcal{U}_{k_F}$ and the ratio of Fermi energy and detuning. Figure 6(b) schematically shows the areas in the parameter space detuning—the Fermi energy where state-filling effect or Hartree-Fock effect dominate: in agreement with Eqs. (16) and (18) the Hartree-Fock contribution dominates at small Fermi energies and high detunings.

Our estimations show that for experimental parameters: $E_g - \hbar\omega = 18$ meV, $E_F \approx 4$ meV ($m = 0.067m_0$, $n = \sqrt{13}$) we get from Eq. (16) $\sigma_F^{\mathrm{sf}} \approx -1.9 \times 10^{-15}$ rad $\times$ cm^2 and from Eq. (18) $\sigma_F^{\mathrm{HF}} \approx 1.2 \times 10^{-15}$ rad$\times$cm^2. The close magnitudes

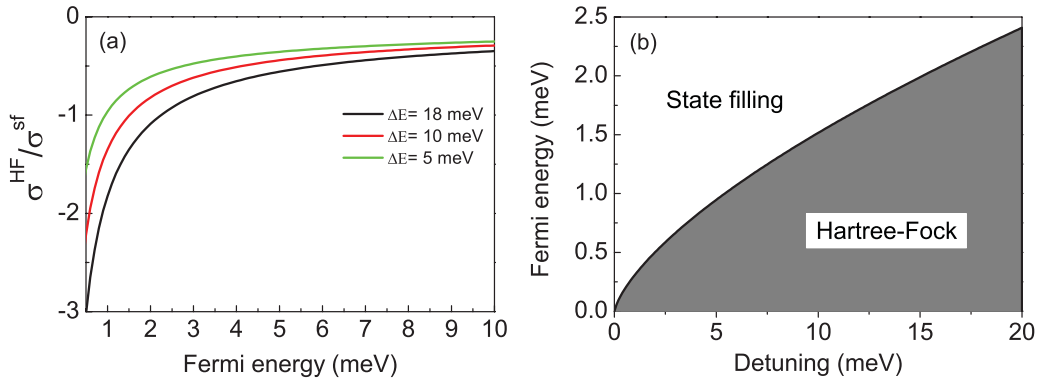

FIG. 6. (Color online) (a) Ratio of Hartree-Fock and state-filling contributions to the Faraday rotation cross section as function of electron Fermi energy, calculated as functions of detuning, ΔE, after Eqs. (18) and (16) respectively. The parameters of GaAs were used. (b) Schematic diagram in the detuning. Fermi energy axes showing dominant contributions to spin Faraday rotation: filled area corresponds to $|\sigma^{\mathrm{HF}}| > |\sigma^{\mathrm{sf}}|$.

of the state-filling effect and Hartree-Fock effect induced Faraday rotation results from the relatively low electron density: In low density electron gas the interaction effects become important. As a result, theoretical estimate for the Faraday rotation cross section is $\sigma_F^{\rm th} = -0.7 \times 10^{-15}$ rad×cm^2. We recall that the negative sign indicates a counterclockwise Faraday rotation when the light propagates along the spin polarization and away from the observer.

C. Experimental determination

1. Photoinduced Faraday rotation

In order to get an experimental estimate of σ_F we use the values of θ_F and ρ_e deduced from photoinduced Faraday rotation and nuclear spin cooling experiments in the same optical pumping conditions (see previous sections). In addition we need to evaluate an effective interaction length inside the microcavity, $d_{\rm eff}$. For a $3\lambda/2$ cavity the interaction length defined as the double thickness of the microcavity $2L$ times the number of round trips $N = Q\lambda_{\rm res}/4\pi L = Q/6\pi$, is $d_{\rm eff} = QL/3\pi$. From interferometric measurements we obtained the quality factor $Q = 19280 \pm 480$, and thus $d_{\rm eff} = 0.7$ mm. Together with the measured value of $\mu = -100^\circ \pm 25^\circ$ (Sec. III), we find the Faraday rotation cross section $\sigma_F = 2\mu/n_e d_{\rm eff} = -(2.5 \pm 0.6) \times 10^{-15}$ rad×cm^2, that is about three times the theoretical value. Bearing in mind that the latter was obtained within a simple model, which neglects electron-hole correlation effects, and using well-known parameters of GaAs, the agreement is reasonable. We note that the main uncertainty in the determination of σ_F comes from the uncertainty in the determination of the electron spin density from the Knight shift. The photoinduced Faraday rotation was found to vary from 19° at the lowest detuning $\Delta = 16$ meV to 14° at the largest detuning $\Delta = 22$ meV. Our results are consistent with the expected inverse detuning dependence of $\sigma_F^{\rm sf}$, but the available detuning range was too small to identify unambiguously the dominant contribution.

2. Field-induced Faraday rotation

In this section we wish to get an independent experimental estimate of the Faraday rotation cross section of the electron gas, from Faraday effect in an external magnetic field applied along the z axis. The external field makes two contributions to the Faraday rotation. The first one is related with the diamagnetic effects, namely, with changes of conduction and valence band orbital states induced by the magnetic field. The second contribution is due to the magnetic field induced (equilibrium) spin polarization of charge carriers.

We found that the diamagnetic effect makes dominant contribution to the field-induced Faraday rotation in our sample. Indeed, we also measured the low-field Faraday rotation from the undoped substrate up to 200 G, and found that it is nearly equal to the Faraday rotation of the whole structure at the same wavelength. Thus, at least in the field range below 200 G the Faraday rotation is entirely dominated by the substrate, which exhibits the expected negative Verdet constant at this wavelength (825 nm).[9]

In order to get rid of these effects, we extract the temperature-dependent contribution by measuring θ_F at different temperatures 2 K up to 20 K [Fig. 7(a)]. In this temperature range one can ignore the temperature dependence of band structure parameters,[31] hence we assume that variations of Faraday rotation angle with temperature reflects those of electron spin polarization.

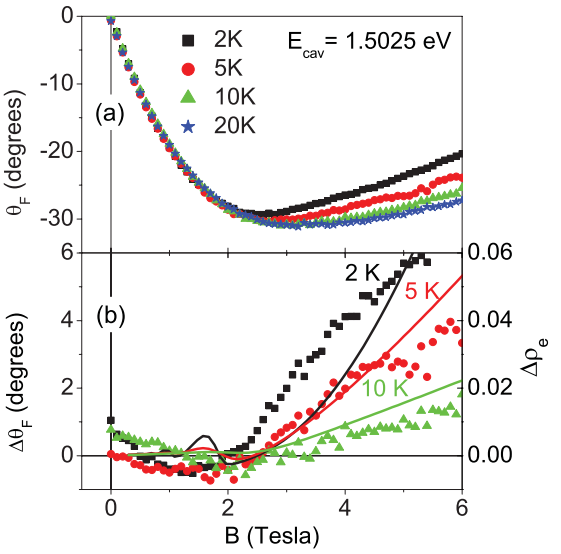

FIG. 7. (Color online) (a) Experimentally measured temperature-dependent Faraday rotations as function of magnetic field at different temperatures: θ_F^{2K} (solid squares), θ_F^{5K} (solid circles), θ_F^{10K} (solid triangles), θ_F^{20K} (solid stars). (b) Comparison between measured Faraday rotation $\Delta\theta_F$ (left scale, symbols) and calculated temperature dependent spin polarization $\Delta\rho_e^{2K}$, $\Delta\rho_e^{5K}$, $\Delta\rho_e^{10K}$ (right scale, lines).

Figure 7(b) shows the differences $\Delta\theta_F^T$ between θ_F^T measured at different temperatures below 20 K, and θ_F^{20K}. One can see that at low field $\Delta\theta_F^T$ remains almost constant and starts to increase at $B > 2$ T [Fig. 7(b)]. Assuming that the temperature-dependent Faraday rotation angle is solely determined by the electron spin polarization, this can be understood as follows.

The equilibrium electron spin induced by magnetic field can be found by a standard method.[33] We take into account that the dispersion of electrons with spin z component $\pm 1/2$ writes $E_\pm(k_z, n_L) = \hbar^2 k_z^2/(2m) + \hbar\omega_C(n_L + 1/2) \pm g\mu_B B/2$, where k_z is the wave vector of electrons along the magnetic field, n_L is the Landau level number and $\omega_C = |e|B/(mc)$ is the cyclotron frequency. In GaAs, the Landau level energy separation exceeds by far the Zeeman splitting, $\hbar\omega_C/(|g|\mu_B B) \approx 60$. The electrons in each spin branch of each Landau level are distributed in accordance with the Fermi-Dirac function $f(E) = \{\exp[(E - \mu(T,B))/(k_B T)] + 1\}^{-1}$, where $\mu(T,B)$ is the temperature- and magnetic field-dependent chemical potential. At zero temperature and in the absence of the magnetic field it coincides with the Fermi energy $\mu(0,0) = E_F$ and for a given electron density can by defined from the condition

$$n_e = \sum_{n_L,\pm} \int \frac{{\rm d}k_z}{2\pi} \mathcal{D}_L f[E_\pm(k_z, n_L)], \qquad (20)$$

where $\mathcal{D}_L = 1/(2\pi l_B^2)$ is the density of states at each Landau level, $l_B = \sqrt{\hbar c/(|e|B)}$ is the magnetic length. The electron spin polarization ρ_e in accordance with Eqs. (3) and (15) is

given by

$$\rho_e = \frac{g\mu_B B}{n_e} \sum_{n_L} \int \frac{dk_z}{2\pi} \mathcal{D}_L f'\left[\hbar\omega_C(n_L + 1/2) + \hbar^2 k_z^2/(2m)\right]. \tag{21}$$

Here $f'(E) = \mathrm{d}f/\mathrm{d}E$ and we took into account the smallness of Zeeman splitting.

In the weak field limit, where $\hbar\omega_C \ll E_F$, $\mu(T,B) \approx \mu(0,0) \equiv E_F$, the summation over Landau levels can be converted in the integration. Therefore under conditions of low field and temperature $\hbar\omega_C \ll E_F, k_B T \ll E_F$ the electron spin polarization reads

$$\rho_e = -\frac{3}{4}\frac{g\mu_B B}{E_F}. \tag{22}$$

The temperature effect in this case is negligible, since for degenerate carriers their equilibrium spin polarization is determined by the ratio of the Zeeman splitting to the Fermi energy. The situation becomes qualitatively different if the magnetic field is so strong that $\hbar\omega_C \gg E_F$ and all electrons occupy the lowest Landau level. Due to singularity of electron density of states at low energies $\mu(T,B) \ll E_F$. Therefore, even at the lowest temperatures $k_B T \sim \mu(0,B)$ and the electron gas becomes nondegenerate. Its spin polarization is given by

$$\rho_e = -\frac{g\mu_B B}{2k_B T}, \tag{23}$$

(i.e., depends strongly on temperature).

The critical magnetic field for the transition between the two regimes can be estimated analytically from the condition $\hbar\omega_C = \mu(0,B) = \hbar^4 n_e/(8me^2\pi B^2)$, assuming that all electrons occupy the lowest Landau level. This yields $B = 1.9$ T, close to the magnetic field at which the temperature dependence shows up in the experiment. In the general case, the dependence of ρ_e on both temperature and magnetic field is calculated numerically and shown in Fig. 7(b).

We get an estimate of the Faraday rotation cross section by scaling the numerically calculated $\Delta\rho_e^T = \rho_e^T - \rho_e^{20K}$ with the experimental $\Delta\theta_F^T$. We introduce the proportionality factor μ_{fi} such that

$$\Delta\theta_F^T = \mu_{\mathrm{fi}} \Delta\rho_e^T. \tag{24}$$

For the calculation of ρ_e^T we assume a degenerate free electron gas, and neglect any eventual field-induced metal to insulator transition, as well as disorder and electron-electron interaction effects. One can see in Fig. 7(b) that a reasonable agreement between experimental Faraday rotation data and calculated spin polarization is obtained for $\mu_{\mathrm{fi}} = 100^\circ$.

From this we deduce $\sigma_F = +2.3 \times 10^{-15}$ rad×cm^2, in reasonable agreement with photoinduced Faraday rotation, excepted for the sign. Indeed, for positive fields the electron spin polarization $\rho_e > 0$ (electron g factor in GaAs is negative), and the corresponding Faraday rotation $\Delta\theta_F^T > 0$, in contradiction with photoinduced Faraday rotation experiments and theoretical predictions. The origin of this discrepancy is not known. Understanding of the temperature dependence of the Faraday rotation in GaAs requires further experimental and theoretical study.

3. Spin noise

Interestingly, one can also estimate σ_F from spin noise spectroscopy experiments. In this case the root-mean-square (RMS) fluctuations of Faraday angle θ_F^{rms} are related to the RMS spin fluctuations of N noninteracting electrons contained in the volume $V = Ad$ probed by the laser, where A is the laser spot area and d is the sample thickness. For noninteracting carriers in equilibrium following the approach of Ref. 33 (see also Ref. 34) one can write for the RMS spin density fluctuation

$$\mathcal{S}_z^{\mathrm{rms}} = \frac{\sqrt{fN}}{2V} = \frac{1}{2}\sqrt{\frac{fn_e}{V}}, \tag{25}$$

where factor

$$f = \frac{\sum_{\boldsymbol{k}} f(\boldsymbol{k})[1 - f(\boldsymbol{k})]}{\sum_{\boldsymbol{k}} f(\boldsymbol{k})} \approx \begin{cases} \frac{3k_B T}{2E_F}, & k_B T \ll E_F, \\ 1, & k_B T \gg E_F, \end{cases}$$

takes into account that only spins in the vicinity of Fermi level can fluctuate. Taking into account that RMS of Faraday rotation angle, θ_F^{rms}, is related with the spin density fluctuation by Eq. (12) one can evaluate Faraday rotation cross section from spin noise data as

$$\sigma_F = \frac{\theta_F^{\mathrm{rms}}}{S_z^{\mathrm{rms}} d} = \frac{2\theta_F^{\mathrm{rms}}}{\sqrt{fn_e}}\sqrt{\frac{A}{d}}. \tag{26}$$

From the measured spin noise power, and the calculated S_z^{rms} we deduced σ_F from two different works[16,32] (see Table I). It turns out that the values of σ_F estimated by spin noise spectroscopy exceed the value estimated by photoinduced Faraday rotation. However, this is consistent with the finding that, at detunings less than 40 meV, Faraday rotation fluctuations due to spin noise increase more rapidly than Faraday rotation induced by a small fixed spin polarization.[16] Since in our

TABLE I. Comparison between measured and calculated Faraday rotation cross sections using either photoinduced or field-induced Faraday rotation (see Sec. IV). Values deduced from spin noise spectroscopy are also given. Calculated values are shown in gray. Note, that in calculation of the Faraday rotation cross section for the spin noise we neglected Hartree-Fock effect, which may be suppressed for localized electrons.

Experiment	Spin polarization ρ_e	Electron density (cm^{-3})	FR θ_F (rad)	Detuning ΔE (meV)	σ_F^{exp} rad×cm^2	σ_F^{th} rad×cm^2
Photoinduced FR (this work)	0.11 ± 0.03	2×10^{16}	0.17	18	$-(2.5 \pm 0.6) \times 10^{-15}$	-0.7×10^{-15}
Field-induced FR (this work)	$\rho_e(B)$	2×10^{16}	$1.75 \times \rho_e(B)$	12	$+2.3 \times 10^{-15}$	-1.05×10^{-15}
Spin Noise[32]	6.8×10^{-6}	1.8×10^{16}	1.2×10^{-5}	25	$\pm 3 \times 10^{-15}$	-1.2×10^{-15}
Spin Noise[16]	8.2×10^{-6}	1.4×10^{16}	10^{-5}	35	$\pm 2.9 \times 10^{-15}$	-0.85×10^{-15}

experiment the spin polarization is created within a 3581-Å thick layer, less than the absorption length, an eventual effect of different spin polarization profiles in both experiments, as invoked in Ref. 16, seems unlikely. The detailed studies of the spin noise magnitudes is beyond the scope of the present paper. To summarize, various estimates of Faraday rotation cross section are given in Table I.

Absolute values of Faraday rotation cross sections estimated by photoinduced Faraday effect, and magnetic field-induced Faraday rotation exceed the theoretical values calculated with Eqs. (16) and (18). Faraday rotation cross sections estimated by spin noise methods are also larger than theoretical predictions of Eq. (16). Also, spin fluctuations seem to induce larger Faraday rotations than a constant macroscopic spin polarization induced optically or by a magnetic field, in agreement with the findings of Crooker *et al.*[16]

VI. TIME-RESOLVED FARADAY ROTATION UNDER PULSED EXCITATION

In this section we show that Faraday rotation can be switched on and off on the nanosecond time scale by weak circularly polarized laser pulses and demonstrate the proof-of-principle of a fast optically controlled Faraday rotator. In these measurements, the magnetic field is not applied.

Figure 8 shows a single-shot time-resolved Faraday rotation sampling, acquired with a fast acquisition card [variant 3 of the setup, Fig. 2(c)] under pumping by a train of laser pulses. At $T = 2$ K the Faraday rotation reaches 13° in about 70 ns, and decays in about 250 ns. The decay time is limited by the electron spin relaxation time. Its value is in reasonable agreement with spin relaxation times deduced from Hanle effect. In contrast, the rise time is determined by the balance between the rate G/n_e, at which electron gas gets spin polarized in the presence of the pump, and the spin relaxation rate. In our experiments the condition $n_e/G \ll \tau_s$ is satisfied. In this strong pumping regime the rise time does not depend on the spin relaxation time and can be much shorter than τ_s.

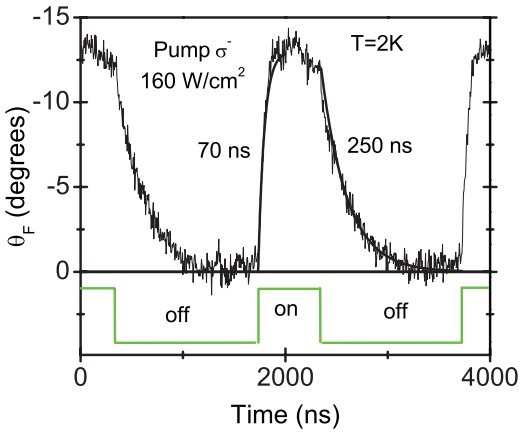

FIG. 8. (Color online) TRFR for circularly polarized 600-ns pulses (open squares). The solid black lines superimposed on experimental data are exponential fits of the rise and decay of the Faraday rotation, and the solid green curve in the figure bottom shows the train of pulses.

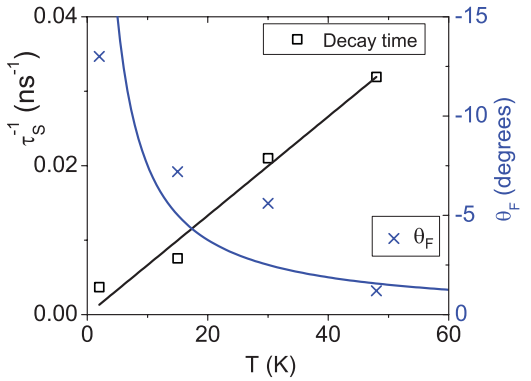

FIG. 9. (Color online) Right scale: Faraday rotation angle (crosses) and its fit (blue line) using Eq. (5) with measured spin relaxation time. Left scale: Temperature dependence of decay time (squares) and its linear fit.

The dependence of the decay rate on the temperature is shown in Fig. 9. Surprisingly we observe linear growth with temperature (solid line in Fig. 9), which is not expected in this temperature range $k_B T < E_F$.[35,20] Further studies are needed to understand this behavior. However, assuming linear growth of the spin relaxation rate with temperature and using Eq. (5) one can reasonably well describe the decay of the Faraday rotation angle when the temperature increases, as shown in Fig. 9. This simple model omits the temperature dependence of the absorption edge (5 meV shift at 50 K) and the eventual change of the quality factor with temperature.

These results show that a high-Q, n-doped microcavity can be an efficient, fast, optically switched Faraday rotator at low temperatures. Much shorter switching times could be reached by using a pair of counterpolarized pump pulses.[36]

VII. CONCLUSION

A high-Q planar $3\lambda/2$ n-doped GaAs microcavity has been used to demonstrate a large Faraday rotation induced by a spin-polarized electron gas. Faraday rotation angles θ_F up to 19° were obtained by optical pumping, and for electron spin polarization ρ_e of only few percents. Independent measurements of θ_F, ρ_e, and Q provide a quantitative determination of the Faraday rotation cross section σ_F, which relates θ_F to the electron spin density, and the thickness of the layer. We found $\sigma_F = -(2.5 \pm 0.6) \times 10^{-15}$ rad $\times$ cm^2 at 18 meV below the band gap, larger than theoretical prediction. The strong negative value of σ_F found experimentally confirms that photoinduced Faraday rotation is dominated by polarization-dependent bleaching of absorption, while spin splitting of conduction band induced by electron-electron interactions, which contribute with the opposite sign, is probably less important.

The comparison of different methods to obtain the Faraday rotation cross section is performed. First, we extracted the electron spin-induced contribution to the Faraday rotation from the temperature dependence of the Faraday effect in the external magnetic field. However, in this experiment the spin polarization cannot be measured directly and is calculated under some poorly controlled assumptions. Therefore, results of field-induced Faraday rotation should be taken with caution.

A similar value was obtained from such an experiment but the sign of extracted θ_F is positive, in contrast to that obtained in theory and by direct experiment. This situation deserves further analysis.

Secondly, we compared the value of σ_F deduced from our measurements, with values deduced from spin noise spectroscopy on n-GaAs bulk layers of comparable electron concentrations. We found that σ_F obtained by spin noise technique exceeds σ_F from photoinduced Faraday rotation. This conclusion agrees with the findings of Crooker *et al.*[16]

Finally, we demonstrate fast optical switching of Faraday rotation in submicrosecond time scale by sampling the Faraday rotation in a one-shot experiment under pulsed excitation. From the decay time of θ_F we deduce the electron spin relaxation time $\tau_s = 250$ ns, slightly longer than the value deduced from Hanle curves $\tau_s = 160$ ns.

ACKNOWLEDGMENTS

We wish to acknowledge the support of the Marie Curie research training network (MC-ITN) Clermont4, Russian Foundation for Basic Research, Dynasty Foundation-International Center for Fundamental Physics in Moscow, and EU Project POLAPHEN. M.N. acknowledges the support from Polish Ministry of Science and Higher Education as research grants. We would like to thank E. L. Ivchenko for critical reading of the manuscript.

[1] L. D. Landau and E. M. Lifshitz, *Electrodynamics of Continuous Media* (Pergamon Press, Oxford, 1984) .

[2] A. K. Zvedin and V. A. Kotov, *Modern Magnetooptics and Magnetooptical Materials* (Institute of Physics, Bristol, 1997) .

[3] P. Kronberg, Rep. Prog. Phys. **57**, 325 (1994).

[4] J. F. Dillon, J. K. Furdyna, U. Debska, and A. Mycielski, J. Appl. Phys. **67**, 4917 (1990); A. Mycielski, L. Kowalczyk, R. R. Galazka, R. Sobolewski, D. Wang, A. Burger, M. Sowinska, M. Groza, P. Siffert, A. Szadkowski, B. Witkowska, and W. Kaliszek, J. Alloys Compd. **423**, 163 (2006).

[5] D. U. Bartholomew, J. K. Furdyna, and A. K. Ramdas, Phys. Rev. B **34**, 6943 (1986).

[6] M. Cardona, Phys. Rev. **121**, 752 (1961).

[7] H. Piller, J. Phys. Chem. Solids **24**, 425 (1963).

[8] H. Piller and V. A. Patton, Phys. Rev. **129**, 1169 (1963).

[9] H. Piller, in *Proceedings of the International Conference on the Physics of Semiconductors* (Academic Press, New York, 1964), p. 297.

[10] L. M. Roth, Phys. Rev. **133**, A542 (1964).

[11] R. Alfano and D. Baird, J. Appl. Phys. **39**, 2931 (1968).

[12] R. K. Willardson and A. C. Beer, *Transport and Optical Phenomena*, Chap. 3 Semiconductors and Semimetals Series, Vol. 8 (Academic Press, New York, 1972).

[13] J. A. Gaj, R. R. Galazka, and M. Nawrocki, Solid State Commun. **25**, 193 (1978).

[14] F. Meier and B. Zakharchenya, *Optical Orientation*, Modern Problems in Condensed Matter Science Series, Vol. 8 (North-Holland, Amsterdam, 1984).

[15] A. Aronov and E. Ivchenko, Sov. Phys.-Sol. State **15**, 160 (1973).

[16] S. A. Crooker, L. Cheng, and D. L. Smith, Phys. Rev. B **79**, 035208 (2009).

[17] A. V. Kavokin, M. R. Vladimirova, M. A. Kaliteevski, O. Lyngnes, J. D. Berger, H. M. Gibbs, and G. Khitrova, Phys. Rev. B **56**, 1087 (1997).

[18] G. Salis and M. Moser, Phys. Rev. B **72**, 115325 (2005).

[19] G. V. Astakhov, M. M. Glazov, D. R. Yakovlev, E. A. Zhukov, W. Ossau, L. W. Molenkamp, and M. Bayer, Semicond. Sci. Technol. **23**, 114001 (2008).

[20] R. I. Dzhioev, K. V. Kavokin, V. L. Korenev, M. V. Lazarev, B. Y. Meltser, M. N. Stepanova, B. P. Zakharchenya, D. Gammon, and D. S. Katzer, Phys. Rev. B **66**, 245204 (2002).

[21] A. I. Ekimov and V. I. Safarov, JETP Lett. **13**, 177 (1971).

[22] M. D. Sturge, Phys. Rev. **129**, 2835 (1963).

[23] Additional contribution to the saturation of the Faraday rotation angle (and electron spin) as a function of pumping power may be related with the onset of Bir-Aronov-Pikus spin relaxation, if density of the photogenerated holes is large enough.[37]

[24] V. Kalevich, V. Kulkov, and V. Fleisher, Bull. Acad. Sci. USSR Phys. Ser. **46**, 70 (1982).

[25] V. Kalevich, V. Kulkov, and V. Fleisher, JETP Lett. **35**, 20 (1982).

[26] D. Paget, G. Lampel, B. Sapoval, and V. I. Safarov, Phys. Rev. B **15**, 5780 (1977).

[27] G. L. Bir and G. E. Pikus, *Symmetry and Deformation Effects in Semiconductors* (Moscow, Nauka, 1972) .

[28] M. M. Glazov and E. L. Ivchenko, JETP **99**, 1279 (2004).

[29] M. M. Glazov, Phys. Solid State **54**, 1 (2012).

[30] E. S. Artemova and I. A. Merkulov, Sov. Phys.-Sol. State **27**, 1558 (1985).

[31] Electron g factor in semiconductors is known to have a temperature dependence.[38–40] Its inclusion may somewhat modify the results for extraction of the electron spin induced contribution to the Faraday rotation in a magnetic field.

[32] M. Römer, J. Hubner, and M. Oestreich, Rev. Sci. Instrum. **78**, 103903 (2007).

[33] L. Landau and E. Lifshitz, *Statistical Physics, Part 1* (Butterworth-Heinemann, Oxford, 2000) .

[34] E. L. Ivchenko, Fiz. Techn. Poluprov. **7**, 998 (1974).

[35] J. M. Kikkawa and D. D. Awschalom, Phys. Rev. Lett. **80**, 4313 (1998).

[36] R. Akimoto, K. Ando, F. Sasaki, and T. Tani, J. Appl. Phys. **84**, 6318 (1998).

[37] R. Völkl, M. Griesbeck, S. A. Tarasenko, D. Schuh, W. Wegscheider, C. Schüller, and T. Korn, Phys. Rev. B **83**, 241306 (2011).

[38] M. Oestreich and W. W. Rühle, Phys. Rev. Lett. **74**, 2315 (1995).

[39] M. Oestreich, S. Hallstein, A. P. Heberle, K. Eberl, E. Bauser, and W. W. Ruhle, Phys. Rev. B **53**, 7911 (1996).

[40] W. Zawadzki, P. Pfeffer, R. Bratschitsch, Z. Chen, S. T. Cundiff, B. N. Murdin, and C. R. Pidgeon, Phys. Rev. B **78**, 245203 (2008).